Met. Mater. Int., Vol. 22, No. 2 (2016), pp. 276~287
doi: 10.1007/s12540-015-4325-x

Application of Central Composite Design for Optimization of Two-Stage Forming Process Using Ultra-thin Ferritic Stainless Steel

Hyuk Jong Bong[1], Frédéric Barlat[1], Jinwoo Lee[2], Myoung-Gyu Lee[3,*], and Jong Hee Kim[4]

[1]Graduate Institute of Ferrous Technology, POSTECH, Pohang, Gyeongbuk 790-784, Korea
[2]Materials Deformation Department, KIMS, Changwon, Gyeongnam 642-831, Korea
[3]Department of Materials Science and Engineering, Korea University, Seoul 136-701, Korea
[4]Stainless Steel Products Research Group, POSCO, Pohang, Gyeongbuk 790-785, Korea

(received date: 2 July 2014 / accepted date: 15 October 2014)

Two-stage forming process for manufacturing micro-channels of bipolar plate as a component of a proton exchange membrane fuel cell was optimized. The sheet materials were ultra-thin ferritic stainless steel (FSS) sheets with thicknesses of 0.1 and 0.075 mm. For the successful micro-channel forming in the two-stage forming approach, three process variables during the first stage were selected: punch radius, die radius, and forming depth. In this study, the effect of the three process variables on the formability of ultra-thin FSSs was investigated by finite element (FE) simulations, experiments, and central composite design (CCD) method. The optimum forming process designed by the CCD showed good agreement with those by experiments and FE simulations. The newly adopted optimization tool, CCD, was found to be very useful for optimization of process parameters in the multi-step sheet metal forming processes.

Keywords: metals, deformation, fracture, finite element method, response surface methodology

1. INTRODUCTION

Of the several material candidates for metallic bipolar plates (BPs), ferritic stainless steels (FSSs) have gained considerable attention owing to their low stack cost compared to other metals, composites, and austenitic stainless steels. In addition, they have good mechanical, electrical, and thermal properties, and workability [1-3]. To reduce the weight of the fuel cell and to make ferritic stainless steel sheets competitive with other materials, the gauge thickness of the BPs should be as thin as possible. However, the forming of an ultra-thin sheet for a BP meets several engineering challenges [4], which include lack of manufacturing process that can provide low cost, high productivity, high precision and robust fabrication. These major technical hurdles must be overcome prior to full commercialization.

Multi-stage forming technology where a final product is formed sequentially in several stamping stages has been utilized to enhance formability of sheet metal parts [5-12]. This technology can also be applied to the forming of ultra-thin sheet material. Since the quality of the final product mostly depends on process parameters, it is necessary to design the most optimum forming process. This is particularly essential for the multi-stage forming which involves more parameters due to the increased forming step. However, the design of the multi-stage forming process frequently relies on engineer's experience, which leads to increased cost and divergence of design qualities [11,13,14]. To overcome this problem, in several previous researches, optimizations of process parameters for the multi-stage forming were conducted by various approaches. For example, Abe *et al.* [10] conducted two-stage cup drawing experiments and relevant finite element (FE) simulations, in which the effect of drawing ratio and punch corner radius on decrease in wall thickness at the first forming stage was investigated. Optimal conditions for the two parameters, i.e., the drawing ratio and the punch corner radius, were determined by comparative study between experiment and FE simulations. Mori *et al.* [6] investigated the shock line formation on the sheet surface during the multi-stage forming of the wheel disk for automotive applications. They simplified the multi-stage forming for the wheel disk as a two-stage forming consisting of deep drawing and unbending. From experiments and complimentary FE simulations for the two-stage forming, they concluded that an increased punch radius at the cup drawing stage and less unbending at the second forming stage are advantageous to remove the shock lines. Suh *et al*. [9] studied the effects of multi-stage forming parameters for U-channel type automobile parts made of ultra-high strength steel sheets. The

*Corresponding author: myounglee@korea.ac.kr,
Hyuk Jong Bong's Present address: Dept. Materials Science and Engineering, The Ohio State University, OH 43210, USA

effect of die angle and direction of punch movement were evaluated, and these parameters were optimized by the FE simulations. The optimization in these researches was mainly based on the comparative studies of experiments and FE simulations. However, this approach leads to increased number of experiments and FE simulations, which in turn increased computational cost. In addition, this approach might be extremely tedious as the number of design variable and forming stage increases.

To efficiently optimize the multi-stage forming processes, a generic algorithm (GA) was adopted by several researchers. Roy *et al.* [5] optimized process parameters such as die geometry, area reduction ratios and the total number of forming stages in cold wire drawing and cold forging with micro GAs. Ko *et al*. [15] also used the GA approach for a multi-stage cold heading process and investigated the effect of process parameters relevant to the process. Tang *et al*. [16] optimized tool shape in the first forming stage of a two-step axisymmetric forming process using GA. However, GA cannot absolutely assure if it finds a global optimum, which often happens when the number of design variable and forming process increases. In addition, the method is not very user-friendly if the users are not well trained for the algorithm. Therefore, devising efficient and user-friendly optimization technique for the multi-stage forming while maintaining high level of accuracy is vital.

Response surface methodology (RSM) proposed by Box and Wilson [17] is a mathematical and statistical technique that can be used for studying the effect of several factors at different levels. Furthermore, it helps to obtain the surface contour that provides an efficient way for visualizing the parameter interaction. The objective of RSM is to optimize the response based on the investigated factors. RSM uses an experimental design such as central composite design (CCD) to fit a model by least square method. Appropriateness of the model is validated using the diagnostic checking tests provided by analysis of variance (ANOVA). The response surface plots can be adopted to study the surfaces and locate the optimum condition. In several industrial processes, RSM has been routinely used to evaluate the results and efficiency of the operations.

The purpose of the present study is two-fold. First, the CCD approach will be introduced in the field of sheet metal forming in order to optimize process parameters in the two-stage forming process for manufacturing micro-channels. To date, the CCD approach has been mainly applied to the field of chemistry, biomedicine and food science where numerous combinations of data should be examined [18-23]. Through the current study, the feasibility and efficiency of the CCD approach for the optimization of the forming process will be sought. Second, the simplicity for users (mainly for field engineers) and its accuracy for the optimization of the multi-stage forming will be discussed based on the results. This study provides optimization results in the two-stage forming process by FE simulation in conjunction with the CCD approach. The results will be also compared with experiments and FE simulations. Since the current study is a preliminary work to validate the accuracy and efficiency of the existing optimization tool, more investigation should be followed as future work, which includes the application of the method to realistic forming process with increased number of process parameters. In this study, the number of the optimized parameters is limited, but the main essence in terms of the theoretical procedure should be the same.

2. TWO-STAGE FORMING PROCESSES FOR MICRO-CHANNEL FORMING

2.1. Material

FSS sheet samples of thickness 0.1 and 0.075 mm were investigated. The sheet material was developed for the application to fuel cell BP. Compared to the conventional chemical composition of FSS, the present material contains nearly 30% Cr for this specific application. With a very strong Cr passive layer, this material has superior corrosion resistance required for the application to the fuel cell BP.

Uniaxial tensile properties of the sheets measured with a Zwick/Roell tensile testing machine are listed in Table 1. The tests were conducted at room temperature and at a constant strain rate of 0.001/s. Test specimens, prepared according to the ASTM E8 standard, were machined with the longitudinal axis aligned with the rolling direction (RD). The Swift hardening equation $\bar{\sigma} = K(\bar{\varepsilon}+\bar{\varepsilon}_0)^n$ was fitted to the experimental stress-strain curve as listed in Table 1.

2.2. Two-stage forming

Two different experimental sets for the two-stage forming were examined; i.e., Case A and B. and the conditions are listed in Table 2. The dimensions of the sample and micro-channel shape after a final stage are shown in Fig. 1(a) and (b), respectively. The values of channel depth and cell pith are not stated in Fig. 1(b) due to confidentiality issues.

All experiments were conducted using a direct-drive digital servo-press, ZENFormer8300DS. The displacement of a slide is directly driven through ball screws by four servo-motors

Table 1. Tensile properties of ferritic stainless steel sheets aligned with RD

Thickness (mm)	0.1	0.075
Elastic modulus (GPa)	200	200
Poisson's ratio	0.3	0.3
Yield Stress (MPa)	398	427
Ultimate Tensile Strength (MPa)	546	584
Uniform Elongation (%)	20.4	21.5
Total Elongation (%)	30.3	29.1
K	1338	1082
$\bar{\varepsilon}_0$	0.01	0.009
n	0.230	0.257

Table 2. Two sets of experiments

Case	Thickness (mm)	Sample dimension	Channel dimension
A	0.1	Fig. 1(a)	Fig. 1(b)
B	0.075	Fig. 1(a)	Fig. 1(b)

and controlled with linear scales attached to the four corners of the slide. The servo-motors independently control positions of the four corners of the slide within ±10 μm accuracy using feed-back from the linear scales. It was decided that the best choice was to adopt the press for the experiments due to high precision of the press.

Two different die sets consisting of a punch and a die cavity were used. A die set with a larger punch radius was used in the first forming stage, whereas a die set for the desired final product design was used in the second forming stage. The forming depth for the micro-channel was prescribed by punch displacement. In the two-stage forming approach, a sheet sample was pre-formed by the first die set. This pre-formed sample was transferred to the second die set, and subsequent forming was conducted to produce final product. All of the experiments were performed without lubrication, and the slide velocity was 1 mm/s.

2.3. Observation of cross-section

The micro-channels formed by the servo-press with the two-stage forming scheme were examined to measure an absolute maximum thickness strain across the micro-channel after the second forming stage, $|\varepsilon_{z'z',max}|$ as an indicator of the formability throughout this study. The parts were cut, and cross-sections of the micro-channels were polished with sand paper. To minimize the effects caused by different machining conditions, samples were always cut at the same spot on the formed sheet and polished the same amount. The cross-sections of the unit micro-channels were observed by an optical microscope.

2.4. Finite element model

A two-dimensional (2D) FE model of the micro-channel forming is shown in Fig. 2. Here, the sheet material is not constrained along micro-channel direction, or directions normal to *x* and *z*. The FE software ABAQUS/Standard was used to simulate the two-stage forming process. The FE model consists of three components: (1) a die, (2) a punch and (3) a sheet blank. The rigid body elements were used for the punch and die. Four channels were modeled and only half of the blank was used considering the symmetry of the micro-channels.

The sheet blank was meshed with 4-node bilinear plane strain quadrilateral elements with reduced integration (CPE4R). The mesh size of 0.01 mm × 0.01 mm for Case A (0.1 mm thick FSS) and 0.0075 mm × 0.0075 mm for Case B (0.075 mm thick FSS) were used. Therefore, 10 elements through the thickness direction were used. For computational simplicity, isotropic elastic-plasticity was assumed for all the simulations in this study.

The die was fixed in all directions and the punch moved following the prescribed displacement boundary condition. The nodes located along the center edge of the sheet blank were fixed in the x-direction of the global coordinate system

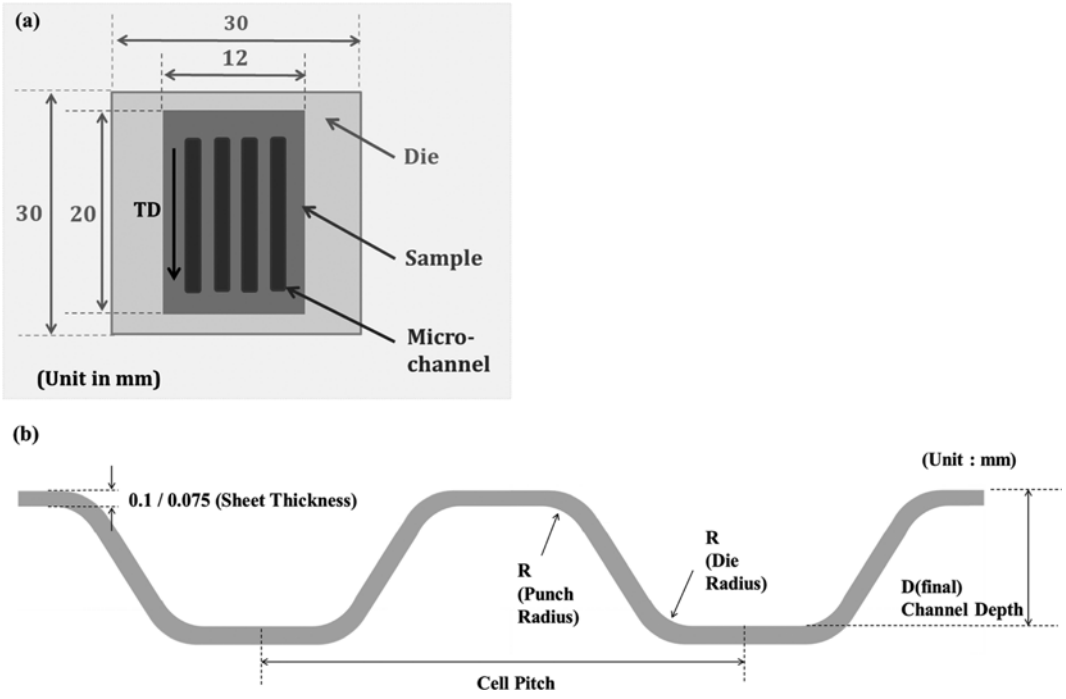

Fig. 1. (a) Sample dimension for two-stage forming and (b) micro-channel dimension.

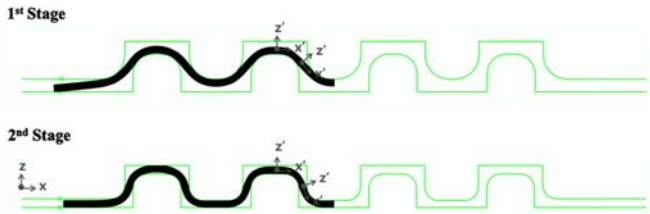

Fig. 2. 2D FE model.

shown in Fig. 2. The nodes can move in the y-direction. There were two contact pairs in the FE model: (a) the die and top surface of the sheet blank and (b) the punch and bottom surface of the sheet blank. The Coulomb's friction law with friction constants of 0.225 for Case A and 0.175 for Case B was assumed.

3. DESIGN OF FE SIMULATION

Note that the terminologies for the CCD approach which appears throughout this paper are defined and summarized in Appendix A. In this study, RSM was based on face-centered CCD with a conceptual framework of full factorial design (FFD). The CCD included an embedded factorial ("cube point") with "center point" and "star points" as depicted in Fig. 3. Three factors during the first forming stage were examined: the punch radius (Factor X_1), the die radius (Factor X_2) and the forming depth, i.e., the pre-forming depth (Factor X_3). For each of the three factors, high (coded level: +1) and low (coded level: -1) set points were selected. Factors and their levels used in the face-centered CCD are listed in Table 3. The same levels were used for Case A and B.

Based on the factors and their levels, a plan for the FE simulation was generated using the statistical software Minitab 17. These values are listed in Table 4 for Case A and Table 5 for Case B. The design for both Cases A and B involves 15 runs, and the response variables at each run were calculated from the FE simulation. The response variable was chosen as $|\varepsilon_{z'z',max}|$. Here, z' is a direction in a local coordinate system depicted in Fig. 2.

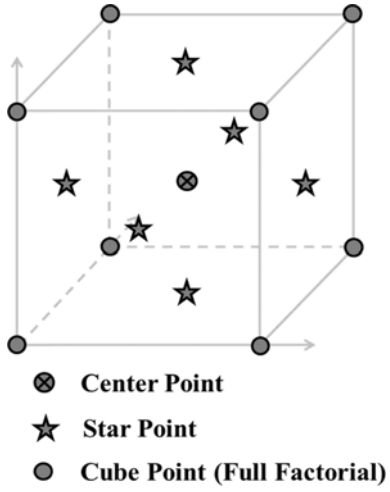

Fig. 3. Face-centered CCD with three variables.

Table 3. Factors and value levels used in face-centered CCD for case A and B

Factors	Low value (coded: -1)	Center value (coded: 0)	High value (coded +1)
X_1	0.25	0.265	0.28
X_2	0.31	0.325	0.34
X_3	0.40	0.45	0.50

Table 4. Design layout and FE simulation results of CCD for case A

Run number	Factor X_1 (uncoded) (unit in mm)	Factor X_2 (uncoded) (unit in mm)	Factor X_3 (uncoded) (unit in mm)	Response Variable, Y
1	0.265	0.34	0.45	0.194
2	0.265	0.31	0.45	0.237
3	0.265	0.325	0.45	0.214
4	0.28	0.34	0.4	0.195
5	0.25	0.34	0.4	0.256
6	0.25	0.31	0.5	0.393
7	0.28	0.31	0.5	0.265
8	0.25	0.34	0.5	0.317
9	0.28	0.34	0.5	0.213
10	0.28	0.31	0.4	0.221
11	0.28	0.325	0.45	0.186
12	0.25	0.325	0.45	0.244
13	0.265	0.325	0.4	0.236
14	0.25	0.31	0.4	0.280
15	0.265	0.325	0.5	0.323

Table 5. Design layout and FE simulation results of CCD for case B

Run number	Factor X_1 (uncoded) (unit in mm)	Factor X_2 (uncoded) (unit in mm)	Factor X_3 (uncoded) (unit in mm)	Response Variable, Y
1	0.265	0.34	0.45	0.194
2	0.25	0.325	0.45	0.249
3	0.265	0.325	0.45	0.213
4	0.265	0.325	0.5	0.338
5	0.28	0.31	0.5	0.267
6	0.265	0.31	0.45	0.238
7	0.25	0.34	0.4	0.196
8	0.28	0.325	0.45	0.181
9	0.265	0.325	0.4	0.293
10	0.25	0.31	0.4	0.207
11	0.25	0.34	0.5	0.351
12	0.28	0.31	0.4	0.259
13	0.28	0.34	0.4	0.236
14	0.28	0.34	0.5	0.197
15	0.25	0.31	0.5	0.378

Table 6. Number of necessary data set for optimization by CCD approach

Number of factors	2	3	4	5	6
Number of data set	9	15	25	49	85

By applying multiple regression analysis on the data, the response variable and the examined factors were related by the following second-order polynomial equation:

$$Y = k_0 + k_1X_1 + k_2X_2 + k_3X_3 + k_{11}X_1^2 + k_{22}X_2^2 + k_{33}X_3^2 + k_{12}X_1X_2 + k_{23}X_2X_3 + k_{13}X_1X_3 \quad (1)$$

where Y is the response variable $|\varepsilon_{z'z',max}|$, k_0 is the offset or constant term, k_1, k_2 and k_3 are the linear effect, k_{11}, k_{22} and k_{33} are the squared effect, k_{12}, k_{23} and k_{13} are the interaction effect.

3.1. Reduced data sets by CCD approach

The number of necessary data sets for optimization by the CCD approach is listed in Table 6. The number of necessary data sets depends on the number of the factors. One of strengths of the CCD approach is that it can dramatically reduce the required data sets for the optimization. For example, only 15 data sets are necessary for the CCD approach for a three-dimensional (3-D) optimization problem like the current problem. If one tries to optimize the 3-D optimization problem by a case-by-case approach without an optimization technique or algorithm, say, with l, m and n discretized levels for each factor, $l \times n \times m$ data sets are necessary. Therefore, required data sets will be significantly increased. In addition, the number will be increased drastically as the number of factor increases. The CCD approach can avoid this tragic situation.

4. RESULTS AND DISCUSSION

4.1. Statistical analysis and model fitting

The second order response surface model (Eq. (1)) was fitted using the analysis of variance (ANOVA) and fitted equation for Case A is as following:

$$Y = 0.2192 - 0.0410X_1 - 0.0221X_2 + 0.0323X_3 - 0.0054X_1^2 - 0.0049X_2^2 + 0.0591X_3^2 + 0.0028X_1X_2 - 0.0098X_2X_3 - 0.0140X_1X_3 \quad (2)$$

Similarly, for Case B:

$$Y = 0.2340 - 0.0242X_1 - 0.0174X_2 + 0.034X_3 - 0.0241X_1^2 - 0.0233X_2^2 + 0.0763X_3^2 + 0.0067X_1X_2 - 0.0078X_2X_3 - 0.0455X_1X_3 \quad (3)$$

The determination coefficient (R^2) was calculated by ANOVA as 0.9825 for Eq. (2) and 0.9743 for Eq. (3). The results indicate that only 1.75% for Case A and 2.57% for Case B were not explained by the model. Therefore, the models were found to be highly significant.

ANOVA determines which of the factors significantly affect the response variable using Fisher's statistical test (F-test) [24]. The significances of the linear, quadratic and interactive terms were digitized for the F-test. The values of the F-test for the determined regression coefficients are listed in Table 7 for Case A and Table 8 for Case B. The p-values are used as a tool to weigh the significance of each coefficient. If the p-value is lower than 0.05, the coefficient is statistically significant [18,22,23]. The results reveal that, for both cases, all of the linear terms (X_1, X_2 and X_3), a quadratic term (X_3) and an interaction term (X_1X_3) are found to be significant with small p-values (<0.05).

4.2. Model validation

A validation of the developed mathematical models was performed to evaluate their accuracy using additional FE simulations with various levels of factors. The two-stage forming conditions for the additional FE simulations were randomly chosen using a uniform probability distribution function within the evaluated level of factors. Five randomly chosen condi-

Table 7. Analysis of variance of Eq. (2)

Source	DF (Degree of freedom)	SS (Sum of square)	MS (Mean of square)*	F-value	p-value
X_1	1	0.01681	0.01681	105.54	0.000
X_2	1	0.00488	0.00488	30.66	0.003
X_3	1	0.01043	0.01043	65.50	0.000
X_1^2	1	0.00007	0.00007	0.48	0.520
X_2^2	1	0.00006	0.00006	0.39	0.557
X_3^2	1	0.00897	0.00897	56.30	0.001
X_1X_2	1	0.00006	0.00006	0.38	0.565
X_2X_3	1	0.00076	0.00076	4.77	0.008
X_1X_3	1	0.00157	0.00157	9.84	0.003
Error	5	0.00080	0.00016		
Total	14	0.04555			

*MS=SS/DF, F-value=MS/MS_{error}

Table 8. Analysis of variance of Eq. (3)

Source	DF (Degree of freedom)	SS (Sum of square)	MS (Mean of square)	F-value	p-value
X_1	1	0.00587	0.00587	21.36	0.006
X_2	1	0.00303	0.00303	11.01	0.021
X_3	1	0.01160	0.01160	42.20	0.001
X_1^2	1	0.00003	0.00003	5.43	0.067
X_2^2	1	0.00001	0.00001	5.08	0.074
X_3^2	1	0.01495	0.01495	54.38	0.001
X_1X_2	1	0.00036	0.00036	1.31	0.303
X_2X_3	1	0.00049	0.00049	1.77	0.240
X_1X_3	1	0.01587	0.01587	57.73	0.001
Error	5	0.00138	0.00028		
Total	14	0.05358			

Table 9. Two-stage forming conditions for addition FE simulation (unit in mm)

Trial number	Case A			Case B		
	X_1 (uncoded)	X_2 (uncoded)	X_3 (uncoded)	X_1 (uncoded)	X_2 (uncoded)	X_3 (uncoded)
1	0.278	0.319	0.411	0.280	0.316	0.460
2	0.272	0.334	0.460	0.260	0.327	0.416
3	0.261	0.316	0.445	0.251	0.325	0.423
4	0.278	0.317	0.470	0.256	0.330	0.411
5	0.266	0.330	0.437	0.255	0.314	0.487

tions for Cases A and B are listed in Table 9. The FE simulations were conducted at the five conditions, and the results were compared with predicted values from the fitted equations (Eqs. (2) and (3)).

Comparisons between FE predicted results and Eqs. (2) and (3) are provided in Fig. 4 for Case A and Fig. 5 for Case B. Predicted response variables from the fitted equations are in good agreement with the results from FE simulations, which resulted in the relative errors of less than 2% for Case A and 3% for Case B. Therefore, strong evidence of accuracy and adequacy of the fitted equations could be guaranteed.

4.3. Visualization of model equations

The response surface plot in a 3D space shows the relationship between the response variable and the independent factors. The 2D display of the surface plot is the contour plot. The plots facilitate the visualization of the shape of the response surface; in turn, they provide useful information on the variation of the response variable with respect to the independent factors.

The generated response surface and contour plots of Eq. (2) for Case A is shown in Fig. 6. The same plots of Eq. (3) is shown in Fig. 6. From Fig. 6(a) and (d), it is apparent that the increase of

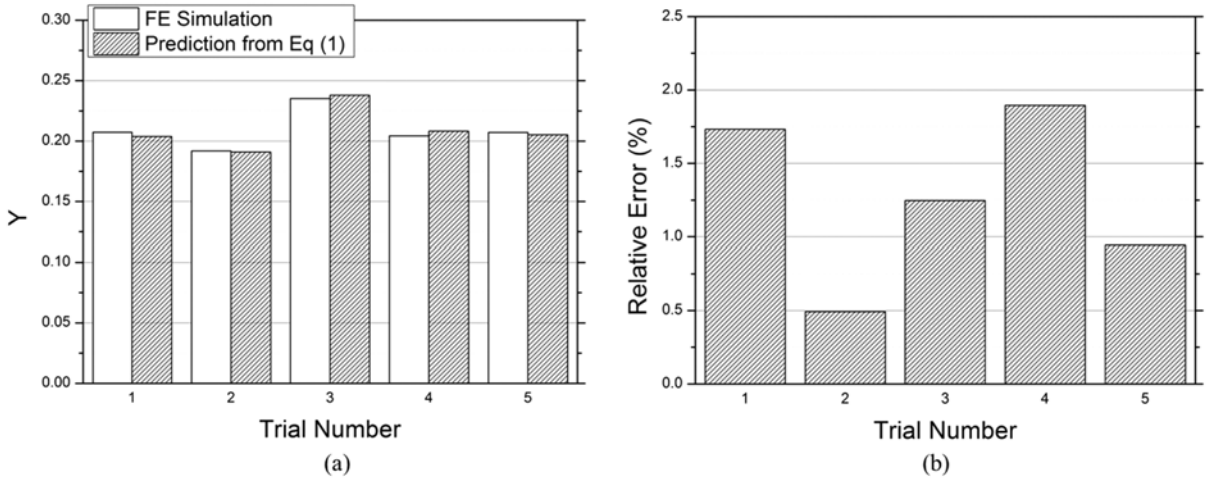

Fig. 4. (a) Comparison of predicted Y by FE Simulation and Eq. for five conditions and (b) relative error of respective trials for case A.

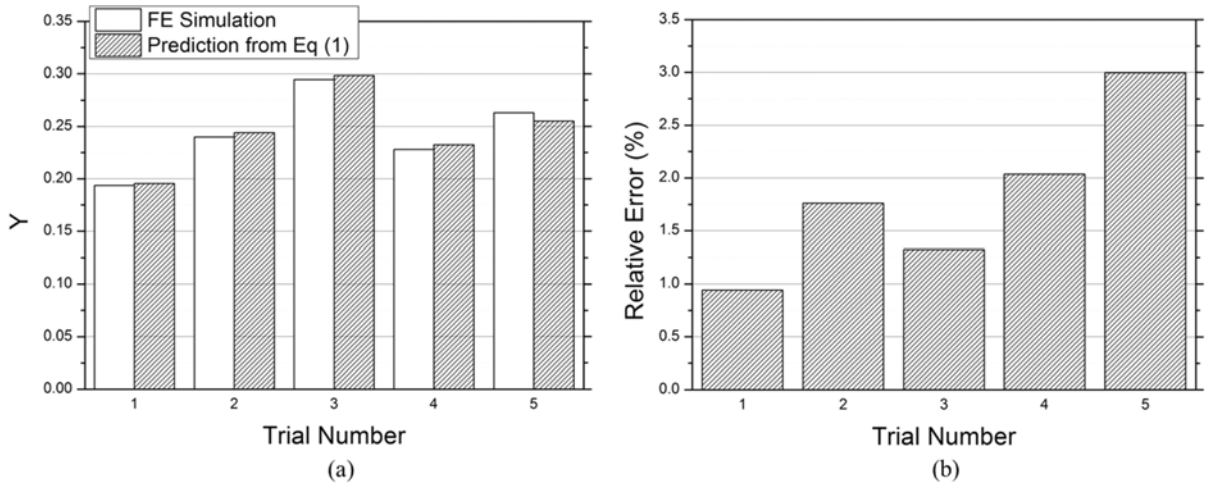

Fig. 5. (a) Comparison of predicted Y by FE Simulation and Eq. (1) for five conditions and (b) relative error of respective trials for case B.

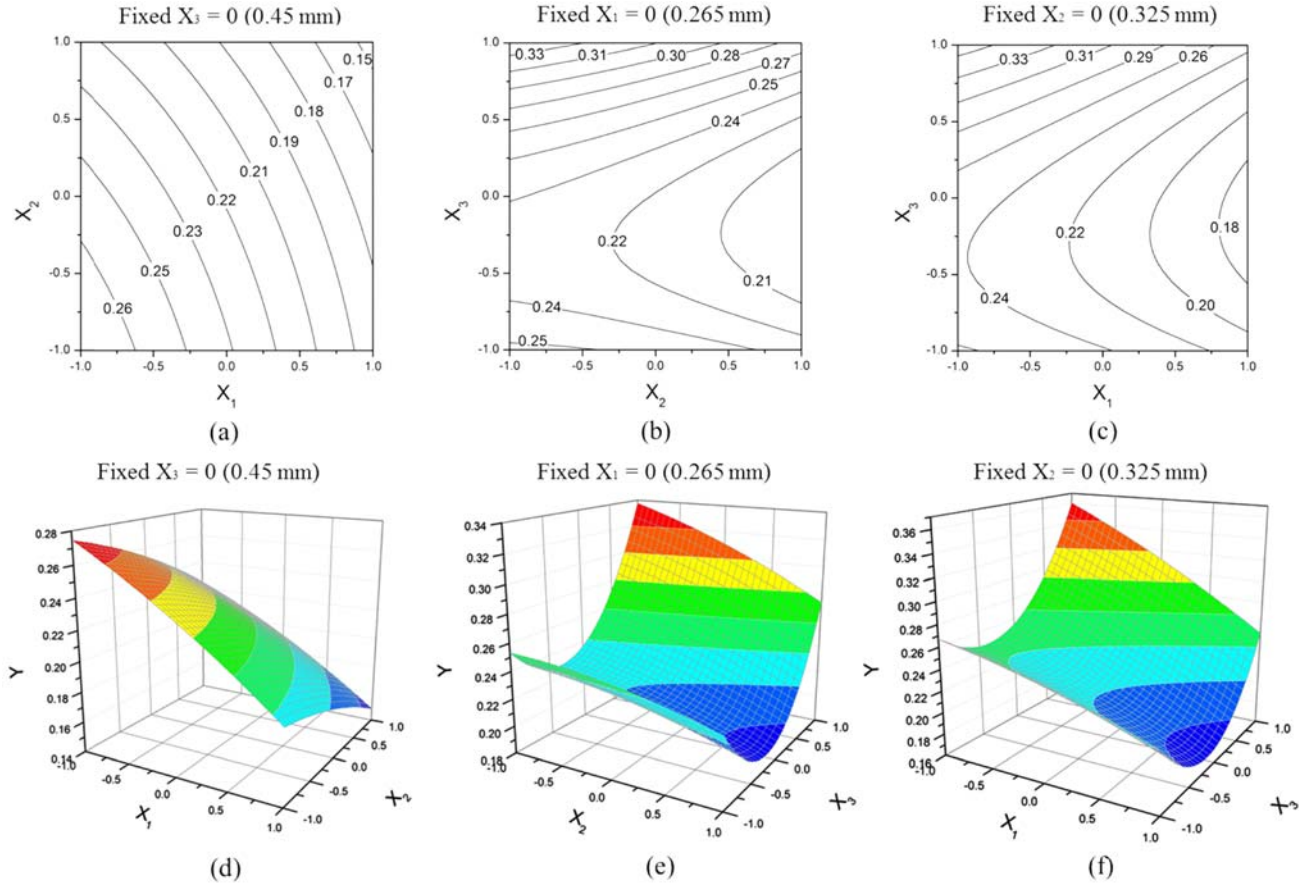

Fig. 6. Contour plots for case A: effect of (a) X_1 and X_2, (b) X_2 and X_3, (c) X_3 and X_1, and surface plots for case A: effect of (d) X_1 and X_2, (e) X_2 and X_3, and (f) X_3 and X_1.

X_1 and X_2 leads to the decrease of Y, or improved formability. In contrast, Figs. 6(d) and (e) show that Y decreases until a certain value of X_3 and increases again as the X_3 increases, regardless of the level of X_1. Additionally, the optimum condition where Y can be minimized is found when X_1 reaches a maximum. Similar results are observed from Figs. 6(c), and (f), where the optimum condition can be found when X_2 reaches a maximum and at certain X_3 value within the evaluated range. A similar trend is observed for Case B, as shown in Fig. 7.

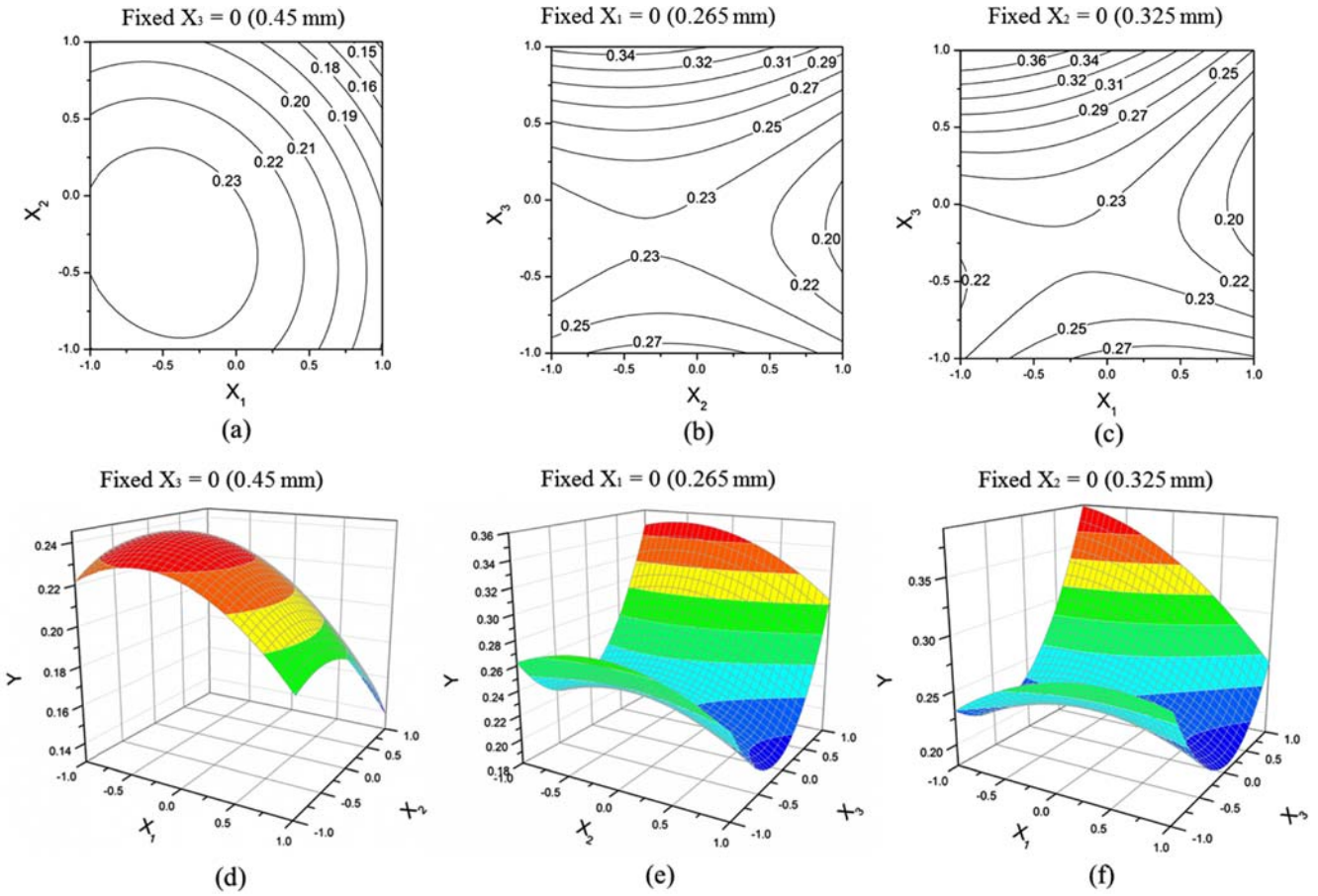

Fig. 7. Contour plots for Case B: effect of (a) X_1 and X_2, (b) X_2 and X_3, (c) X_3 and X_1, and surface plots for case B: effect of (d) X_1 and X_2 (e) X_2 and X_3 (f) X_3 and X_1.

4.4. Optimization

The fitted model equation was used to determine the optimum conditions of the three factors to minimize the response variable *Y*. The obtained optimum conditions are listed in Table 10. In both Cases A and B, the results indicate that the two-stage forming process needs to be designed to maximize the factors X_1 and X_2. In contrast, the optimum X_3 is found to be 0.447 mm for Case A and 0.456 mm for Case B.

To verify the optimized results by the CCD, additional case-by-case FE simulations were performed and compared with the optimization results in Table 10. Since considering all the factors in FE simulations are highly laborious and time-consuming, the factors X_1 and X_2 were fixed as determined values in Table 10 and only the factor X_3 was varied as discrete values from 0.4 to 0.5. The results were compared with the fitted model equations, and the comparison is shown in Fig. 8.

Table 10. Optimization results (unit in mm)

Factor	Case A (uncoded)	Case B (uncoded)
X_1	0.28 (max)	0.28 (max)
X_2	0.34 (max)	0.34 (max)
X_3	0.447	0.456

The results of the two approaches are well matched for both cases and show the same trend, i.e., a parabolic shape. Based on the results by the case-by-case FE simulations, the optimum values are found to be 0.455 mm for Case A and 0.465 mm for Case B. The relative error of the optimum X_3 value with respect to the case-by-case FE simulations is less than 2% regardless of the cases as listed in Table 11.

In addition to the verification by FE simulations, experiments were also conducted with several X_3 values. In this approach, the factor X_1 and X_2 were also fixed as determined values in Table 10. Three tests were carried out for each process parameter X_3 and the results were averaged. The cross-sections of the formed parts were measured following the procedure described in Section 2.3. The experimentally measured $|\varepsilon_{z'z',max}|$ was compared with the fitted model equations. The comparison is shown in Fig. 9. Experimental results follow a similar trend with good agreement with the CCD results for both cases. Based on the experimental results, the values for optimum X_3 are determined as 0.448 mm for Case A and 0.470-0.493 mm for Case B. The optimization by the CCD approach seems to be successful for the prediction of experimental X_3 value with the relative error of 0.2% for Case A

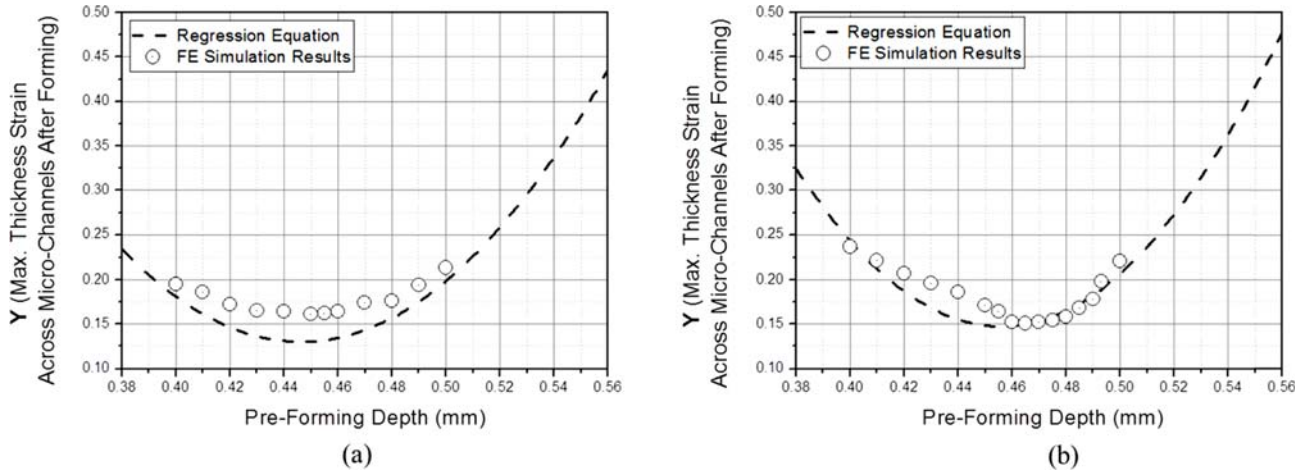

Fig. 8. Comparison of determined model equation by CCD and additional FE simulations at various X_3 when X_1 and X_2 are fixed as their maximum, 0.28 and 0.34 mm, respectively, for (a) case A and (b) case B.

Table 11. Relative error of optimization results by CCD

Relative Error in optimum X_3	Case A (uncoded)	Case B (uncoded)
To case-by-case FE simulations (%)**	1.75	1.94
To experiments (%)***	0.22	2.98-7.50

**Determined optimum X_3 = 0.455 and 0.465 mm for Case A and Case B, respectively (from Fig. 8)
***Determined optimum X_3 = 0.448 and 0.470-0.493 mm for Case A and Case B, respectively (from Fig. 9)

and 3~7% for Case B as listed in Table 11.

4.4.1. Optimization with various boundaries of factors

In the optimization problem, a choice of different boundary conditions (BCs) of the factors may not lead to analogous optimization results. To confirm the reliability and robustness of the optimization results by the current CCD approach, the optimization with various BCs of the factors was perform. Only Case A was considered for this analysis. The applied BCs are listed in Table 12. The results were compared with the optimum values in Table 10. Optimization results (unit in mm). The compared results are also shown in Fig. 10. Figure 10(a) shows the determined optimum levels of factors with various BCs. Among 10 BCs, BC1 corresponds to the reference BC in this study (same as in Table 3). From the results two aspects can be observed. First, the CCD gives identical optimized values of X_1 = 0.28 mm (maximum) and X_2 = 0.34 mm (maximum). Second, the CCD gives similar optimum values of X_3. The determined optimum X_3 with various BCs was compared with the optimum X_3 for Case A in Table 10 (an optimum X_3 at the reference BC). The relative error calculated from the comparison is shown in Fig. 10(b). Regardless of the BCs, the determined X_3 values are not significantly different with the relative error less than 3.5%. Therefore, the

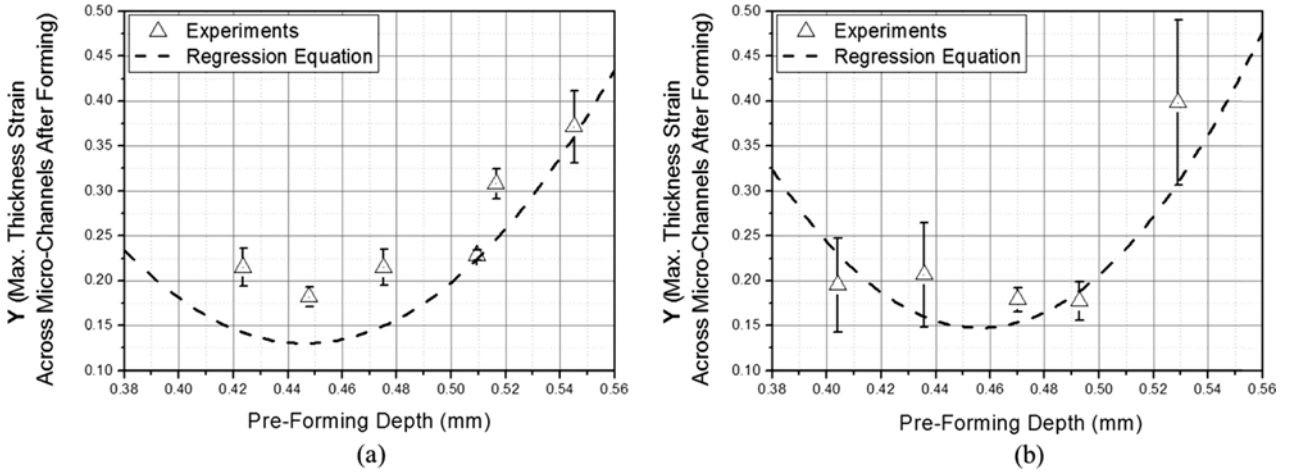

Fig. 9. Comparison of determined model equation by CCD and experiments at various X_3 when X_1 and X_2 are fixed as their maximum, 0.28 and 0.34 mm, respectively, for (a) case A and (b) case B.

Table 12. Boundary conditions of factors for optimization

	X_1		X_2		X_3	
Boundary Condition	Lowest (mm)	Highest (mm)	Lowest (mm)	Highest (mm)	Lowest (mm)	Highest (mm)
1****	0.23	0.28	0.31	0.34	0.40	0.50
2	0.25	0.28	0.29	0.34	0.40	0.50
3	0.23	0.28	0.29	0.34	0.40	0.50
4	0.25	0.28	0.31	0.34	0.38	0.50
5	0.25	0.28	0.31	0.34	0.40	0.52
6	0.25	0.28	0.31	0.34	0.38	0.52
7	0.25	0.28	0.31	0.34	0.42	0.50
8	0.25	0.28	0.31	0.34	0.40	0.48
9	0.25	0.28	0.31	0.34	0.42	0.48
10	0.25	0.28	0.31	0.34	0.38	0.48

****Reference boundary condition in this study (same as in Table 3. Factors and value levels used in face-centered CCD for Case A and B)

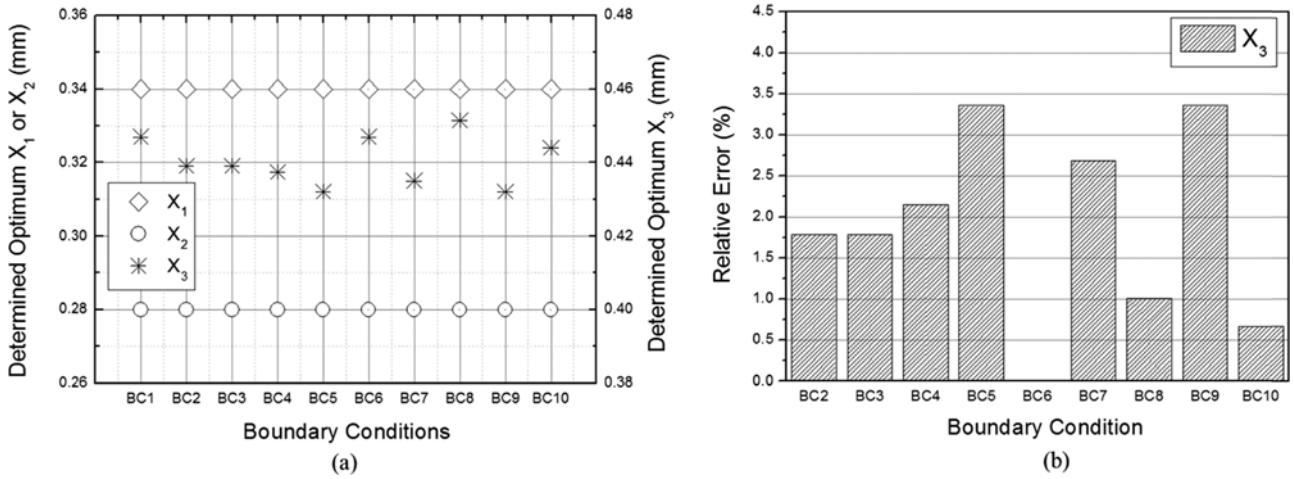

Fig. 10. (a) Optimized factors with various BCs and (b) relative error between optimized X_3 values with various BCs and X_3 value with reference BC in Table 3 for case A.

robustness of the current CCD technique can be guaranteed in regard to the various BCs for this particular application.

4.5. Iso-error map of the developed model by CCD

To evaluate the accuracy and the feasibility of the developed model with more rigorous manner, an iso-error map [25] was generated for Case A, as shown in Fig. 11. Note that this iso-error map concept has been frequently used to evaluate the accuracy of the numerical algorithm for elasto-plastic stress update scheme. The relative absolute error between the calculated Y from Eq. (2) and the exact Y was used as below.

$$Error = \left| \frac{Y_{model} - Y_{exact}}{Y_{exact}} \right| \times 100 \quad (4)$$

Because the experimental results were limited, the calculated Y from additional FE simulations was assumed as Y_{exact}.

The additional FE simulations were conducted on the same conditions in Fig. 6, i.e., X_1 and X_2 plane for a constant $X_3 = 0.45$ mm, X_2 and X_3 plane for a constant $X_1 = 0.265$ mm, and X_1 and X_3 plane for a constant $X_2 = 0.325$ mm. The FE simulations were conducted with combinations of two factors in 7 by 7 matrix while the other factor was fixed. The conditions are listed in Table 13.

In Figure 11, the results show that the determined model equation by the CCD gives accurate prediction within the error of less than 8% throughout the whole region.

5. CONCLUSION

The two-stage forming process for the 0.1 and 0.075 mm thick ultra-thin ferritic stainless steel (FSS) sheets was optimized by a mathematical and statistical technique, CCD method. To achieve successful micro-channel forming, tries were made to minimize the response variable, absolute maximum thickness strain across the micro-channel after the second forming stage, by examining the best combination of the three process variables (factors) during the first forming stage: punch radius, die radius, and forming depth (pre-form-

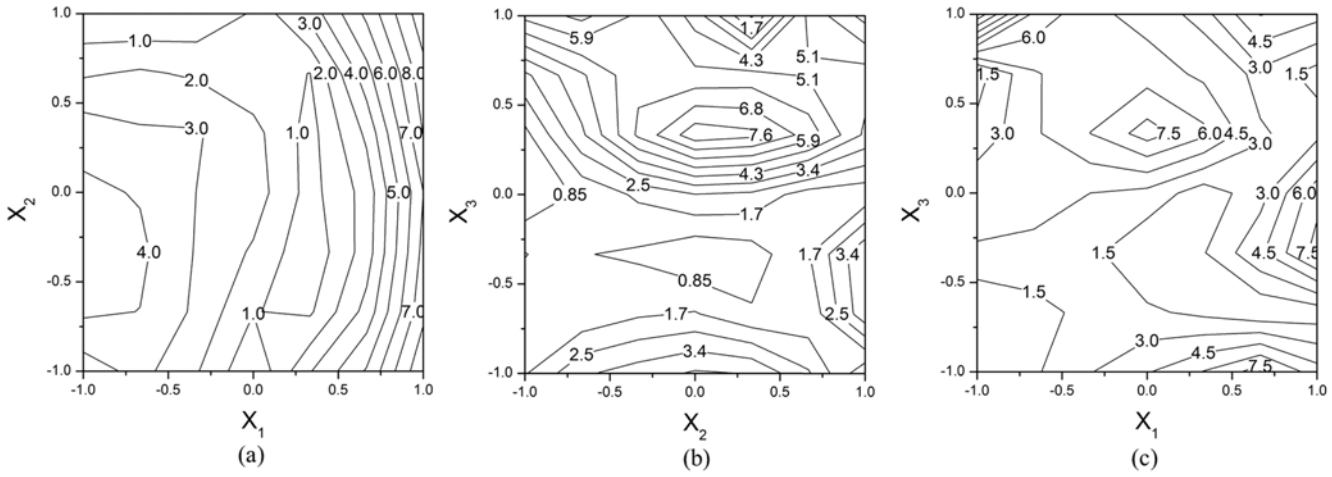

Fig. 11. Iso-error map of (a) X_1 and X_2, (b) X_2 and X_3, and (c) X_3 and X_1 for case A.

Table 13. Condition for generation of iso-error map in case A (unit in mm)

Factor	Fig. 11(a)	Fig. 11(b)	Fig. 11(c)
X_1	0.25~0.28 (interval: 0.005)	0.265 (fixed)	0.25~0.28 (interval: 0.005)
X_2	0.31~0.34 (interval: 0.005)	0.31~0.34 (interval: 0.005)	0.325 (fixed)
X_3	0.45 (fixed)	0.4~0.5 (interval: 0.033)	0.4~0.5 (interval: 0.033)

ing depth). Based on the optimization results by the CCD approach and its complementary finite element (FE) simulations and experiments, the followings could be concluded.

(1) The FE optimized results from the CCD predicted that larger punch and die radii at the first forming stage were effective for enhancing the formability of ultra-thin FSS sheet micro-channels. Moreover, an optimum pre-forming depth existed within the evaluated level where the formability could be maximized for both sheets.

(2) The fitted model equation determined from the CCD and ANOVA was validated using additional FE simulations with randomly chosen process conditions. The FE results correlated well with the CCD model.

(3) The optimized process parameters for the two-stage forming process from the CCD were in good agreement with those from the case-by-case FE simulations and from experiments

(4) All of the approaches, i.e., CCD based FE simulation, case-by-case FE simulations, and experiments at fixed punch and die radii at the first forming stage, showed that an optimum value of pre-forming depth existed within the evaluated level.

(5) The optimized pre-forming depth by the CCD approach with fixed punch and die radii (one-dimensional optimization problem) was in good agreement with both case-by-case FE simulations and experiments. Therefore, reliability and accuracy of the CCD was guaranteed for the one-dimensional optimization problem.

(6) The accuracy of the CCD with dramatically reduced number of experiments or FE simulation data for the optimization was demonstrated.

(7) The robustness of the optimization results in regard to boundary conditions (BCs) in the CCD approach could be confirmed from the optimization results with various BCs.

(8) The accuracy of the determined model from the CCD was demonstrated by the iso-error map analysis.

(9) The investigation in this study opened up opportunities for the application of the CCD optimization techniques to the sheet metal forming field by taking advantage of their accuracy, simplicity and flexibility.

ACKNOWLEDGMENTS

Authors acknowledge J.-H. Choi for his helps for the experiment, POSCO for their financial support and S.W. Kwon at Sungwoo for his technical helps. This research was also supported by the National Research Foundation of Korea (NRF) Grant funded by MSIP (NRF-2012R1A5A1048294) and a grant (NRF-2014R1A2A1A11052889). MGL appreciates support from Korea University Grant.

REFERENCES

1. J.-B. Lee and I. Oh, *Met. Mater. Int*. **20**, 629 (2014).
2. C.-H. Park and K.-H. Baik, *Met. Mater. Int*. **20**, 63 (2014).
3. H. R. Park, *Korean J. Met. Mater*. **52**, 421 (2014).
4. H. J. Bong, F. Barlat, M. G. Lee, and D. C. Ahn, *Int. J. Mech. Sci.* **64**, 1 (2012).
5. S. Roy, S. Ghosh, and R. Shivpuri, *Int. J. Mach. Tool. Manu.* **37**, 29 (1997).

6. K. Mori, Y. Abe, and O. Ebihara, *Int. J. Mach. Tool. Manu.* **43**, 1279 (2003).
7. W. Chen, Z. J. Liu, B. Hou, and R. X. Du, *J. Mater. Process. Tech.* **187-188**, 113 (2007).
8. M. Skjoedt, M. B. Silva, P. A. F. Martins, and N. Bay, *J. Strain. Anal. Eng.* **45**, 33 (2010).
9. C. H. Suh, Y. C. Jung, Y. H. Lim, H. Yun, K. Lee, and Y. S. Kim, *Tran. of the KSME (A)* **36**, 283 (2012).
10. Y. Abe, K. Mori, and O. Ebihara, *J. Mater. Process. Tech.* **125-126**, 792 (2002).
11. S. H. Kim, S. H. Kim, and H. Huh, *J. Mater. Process. Tech.* **113**, 766 (2001).
12. J. H. Noh and B. B. Hwang, *Met. Mater. Int.* **19**, 1193 (2013).
13. W. Chen, J. C. Yang, and Z. Q. Lin, *Int. J. Mach. Tool. Manu.* **42**, 1195 (2002).
14. H. S. Choi, K. J. Nam, W. S. Lim, D. C. Ko, and B. M. Kim, *Met. Mater. Int.* **16**, 1001 (2010).
15. D.-C. Ko, D.-H. Kim, and B.-M. Kim, *Int. J. Mach. Tool. Manu.* **39**, 771 (1999).
16. Y.-C. Tang, X.-H. Zhou, and J. Chen, *Finite. Elem. Anal. Des.* **44**, 462 (2008).
17. G. E. P. Box and K. B. Wilson, *Journal of Royal Statistical Society, Series A (General)* **13**, 1 (1951).
18. N. Sarlak, M. A. F. Nejad, S. Shakhesi, and K. Shabani, *Chem. Eng. J.* **210**, 410 (2012).
19. I. Xiarchos, A. Jaworska, and G. Zakrzewska-Trznadel, *J. Membrane. Sci.* **321**, 222 (2008).
20. A. G. Liew Abdullah, N. M. Sulaiman, M. K. Aroua, and M. J. Megat Mohd Noor, *J. Food. Eng.* **81**, 65 (2007).
21. A. R. Khataee, M. Fathinia, S. Aber, and M. Zarei, *J. Hazard. Mater.* **181**, 886 (2010).
22. Y. Sun, J. Liu, and J. F. Kennedy, *Carbohyd. Polym.* **80**, 949 (2010).
23. P. A. J. Rosa, A. M. Azevedo, and M. R. Aires-Barros, *J. Chromatogr. A* **1141**, 50 (2007).
24. R. A. Fisher, *J. R. Stat. Soc.* **85**, 87 (1922).
25. J. Lee, M.-G. Lee, F. Barlat, and J. H. Kim, *Comput. Method. Appl. M.* **247-248**, 73 (2012).

Appendix A

Terminologies in the CCD approach are defined and briefly described as following.

Factor: process parameter

Level: specific value of factors

Responds variable: measured output at various combinations of levels and factors.

Uncoded level: real level of factor

Coded level: -1 for the lowest uncoded level, +1 for the highest uncodede level, and 0 for a central uncoded level.

Full factorial design (FFD): an experimental design with all input factors set at the highest and lowest levels. It corresponds to face-centered CCD only with cube point in Fig. 3. Face-centered CCD with three variables (without star and center points).

Run: a test at a given test condition.